AIAA Atmospheric Flight Mechanics Conference and Exhibit
15 - 18 August 2005, San Francisco, California

AIAA 2005-6331

Lateral-Directional Aircraft Dynamics at High Incidence Flight with Account of Unsteady Aerodynamic Effects

N. Abramov [*], M. Goman [†], M. Demenkov [‡] and A. Khrabrov [§]

De Montfort University, Leicester, LE3 9BH, UK

Central Aerohydrodynamic Institute (TsAGI), Zhukhovsky, 140180, Russia

A traditional representation of aerodynamic characteristics based on the concept of aerodynamic derivatives becomes inadequate at high angles of attack due to significant dynamic effects generated by separated and vortical flow. The main difficulty in an application of aerodynamic derivatives at these conditions is linked with their strong dependence on frequency and amplitude of oscillations. To describe these dependencies the mathematical model for aerodynamic characteristics in the time domain should be dynamic and nonlinear.

To capture frequency effects the lateral/directional aerodynamic characteristics are represented in the form of differential equations and applied for the open- and closed-loop dynamic analysis.

I. Introduction

Representation of aerodynamic coefficients based on the aerodynamic derivatives concept is conventionally used in all engineering flight dynamics applications. The same representation is extended also to high incidence flight conditions by adding nonlinear dependencies obtained in wind tunnel tests using static and rotary balance rigs. However, this approach based on the concept of aerodynamic derivatives becomes inadequate at high angles of attack due to significant dynamic effect from separated and vortical flow. Aerodynamic derivatives may strongly depend on frequency and amplitude of oscillations and this makes it difficult to model aerodynamic coefficients in the time domain.[1]

A general formulation of the aerodynamic characteristics in aircraft dynamics requires inclusion of motion prehistory effects.[2] This is especially important for high angles of attack beyond stall conditions, where flow separation and vortex breakdown processes produce time lag effects significant for rigid body dynamics.

Expanding a flight envelope to high angle of attack can be beneficial for many existing aircraft and also for future ones and UAVs. For example, the experimental aircraft X-31 VECTOR program[3] has recently demonstrated a possibility of an automated landing at angles of attack up to $\alpha = 24^0$. The landing speed was reduced considerably resulting in significantly shorter roll-out distances. Further increase of angle of attack beyond the stall conditions and reduction in landing speed will require for reliable control design solutions an improved aerodynamic modelling technique.

[*] Ph.D., Faculty of Computing Sciences and Engineering, The Gateway
[†] Professor, Faculty of Computing Sciences and Engineering, The Gateway
[‡] Ph.D. Student, Faculty of Computing Sciences and Engineering, The Gateway
[§] Head of Unsteady Aerodynamics Subdivision, Flight Dynamics and Control Department

A simple modelling method for unsteady nonlinear aerodynamic characteristics based on an application of dynamical models has been proposed and studied in.[5,6,7,8,9] The frequency dependant in-phase and out-phase aerodynamic derivatives obtained in conventional wind tunnel forced oscillations tests can be simulated by unsteady aerodynamic model in the form of linear first order differential equations with characteristic time constants specifying the internal flow time lag effects. This unsteady aerodynamic model generates aerodynamic loads with the identical to experimentally obtained frequency dependant aerodynamic derivatives. At angles of attack $\alpha \geq 25^0$ beyond the stall conditions the characteristic time scales identified in paper[9] for the X-31 aircraft equal $(15 \div 20)\dfrac{\bar{c}}{V}$ allow the linear unsteady aerodynamic model to fit the experimental aerodynamic derivatives[4] very accurately as shown in Fig.2. The frequency effect in aerodynamic derivatives is getting stronger above $\alpha \geq 25^0$ and should be adequately accounted for in dynamics analysis, while below $\alpha < 25^0$ this effect is not significant and the conventional aerodynamic derivatives model for representation of aerodynamic coefficients is acceptable.

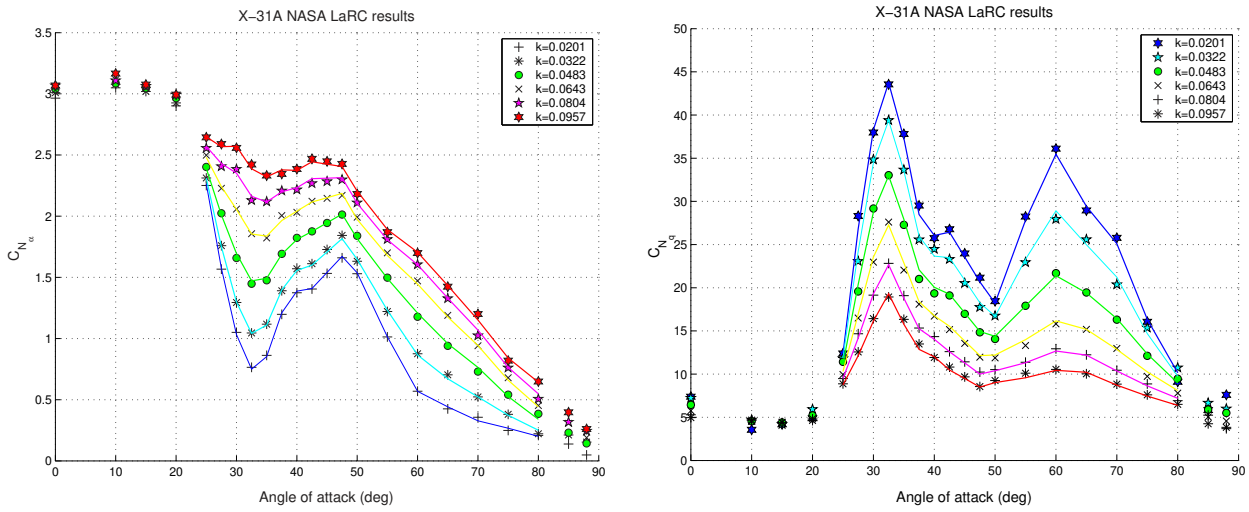

(a) In-phase derivative $C_{N_\alpha}(\alpha)$

(b) Out-of-phase derivative $C_{N_q}(\alpha)$

Figure 1. Predicted and experimental dependencies for the X-31 aircraft normal force aerodynamic derivatives[4,9].

The paper[11] reported about comparative analysis of the aircraft longitudinal dynamics at high incidence flight considering two forms of aerodynamics representation, the conventional one based on the aerodynamic derivatives concept and the unsteady aerodynamic model taking into account internal flow time lag effects.

This paper as an extension of[11] is presenting comparative analysis of the aircraft lateral/directional motion considering these two forms of aerodynamic models. The same hypothetical aircraft model based on the 65^0 delta wing and thrust vectoring control has been accepted in this paper as a case study (Fig.2,a).

The experimental investigation carried out in 1999-2001 in TsAGI, Russia with support from DERA, UK has provided a comprehensive set of static and dynamic wind tunnel data for the 65^0 delta wing (Fig.2,b). A simple representation of aerodynamic characteristics based on an application of dynamical models and available experimental data has been developed for the longitudinal and lateral/directional motion modes.[8,9]

The Dutch-roll, roll-subsidence and spiral modes are analyzed in terms of coupling with unsteady aerodynamic eigenvalues generated at high incidence by internal vortical and separated flow dynamics. It is demonstrated that the results of the open-loop stability analysis for the conventional aerodynamic derivatives based model and unsteady aerodynamic model at some angles of attack can differ significantly. Control

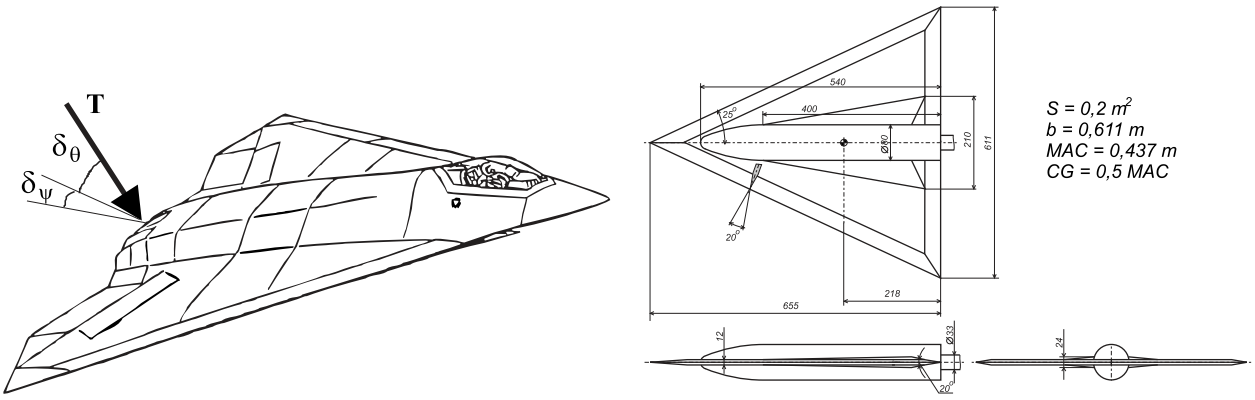

(a) An all-wing tailless concept employing a 65^0 sweep delta wing[12]

(b) The 65^0 delta wing tested in TsAGI low speed wind tunnel[8,9]

Figure 2. A hypothetical 65^0 delta wing aircraft model with thrust vectoring.

law design issues with combination of aerodynamic and thrust vectoring control are also discussed considering linear and nonlinear problem formulation.

II. Mathematical models of the rolling and yawing moment coefficients

A. Conventional aerodynamic derivatives representation

Aerodynamic effects in the lateral/directional moments and side force due to rotation and change of sideslip is normally described in the form of aerodynamic derivatives. Unsteady aerodynamic derivatives due to $\beta' = \dfrac{\dot{\beta} b}{2V}$ are commonly combined with the rotary derivatives with respect to reduced angular rates $p' = \dfrac{pb}{2V}$ and $r' = \dfrac{rb}{2V}$ in a form they are extracted from the forced oscillation tests. This aerodynamic representation is rather accurate at low angles of attack, where aerodynamic loads are practically linear functions of kinematic parameters and their derivatives do not depend on frequency of oscillations. It is a conventional form for dynamics simulation and stability analysis at normal flight conditions.

Extension of the linear derivatives representation to high angles of attack regimes is normally attained by a formal inclusion of nonlinear static terms and making aerodynamic derivatives dependent on angle of attack and sideslip:

$$C_i = C_{i_{st}}(\alpha,\beta) + C_{i_{p_{f.o.}}}(\alpha,k)\frac{pb}{2V} + C_{i_{r_{f.o.}}}(\alpha,k)\frac{rb}{2V} + C_{i_{\delta_a}}(\alpha)\delta_a \tag{1}$$

where $i = l, n, Y$, b is the wing span, $f.o.$ stands for forced oscillations, $k = \dfrac{\omega b}{2V}$ is reduced frequency.

The static term in (1) is essentially nonlinear at high angles of attack $\alpha = 20 \div 40^0$ and also very sensitive to wing motion. The nonlinear steady aerodynamic loads become very coupled with unsteady aerodynamic contributions and are directly associated with dependence of the aerodynamic derivatives on frequency. However, in modelling with (1) the dependence on reduce frequency k is usually ignored as it is very difficult to specify k in the time domain during non-periodic motion.

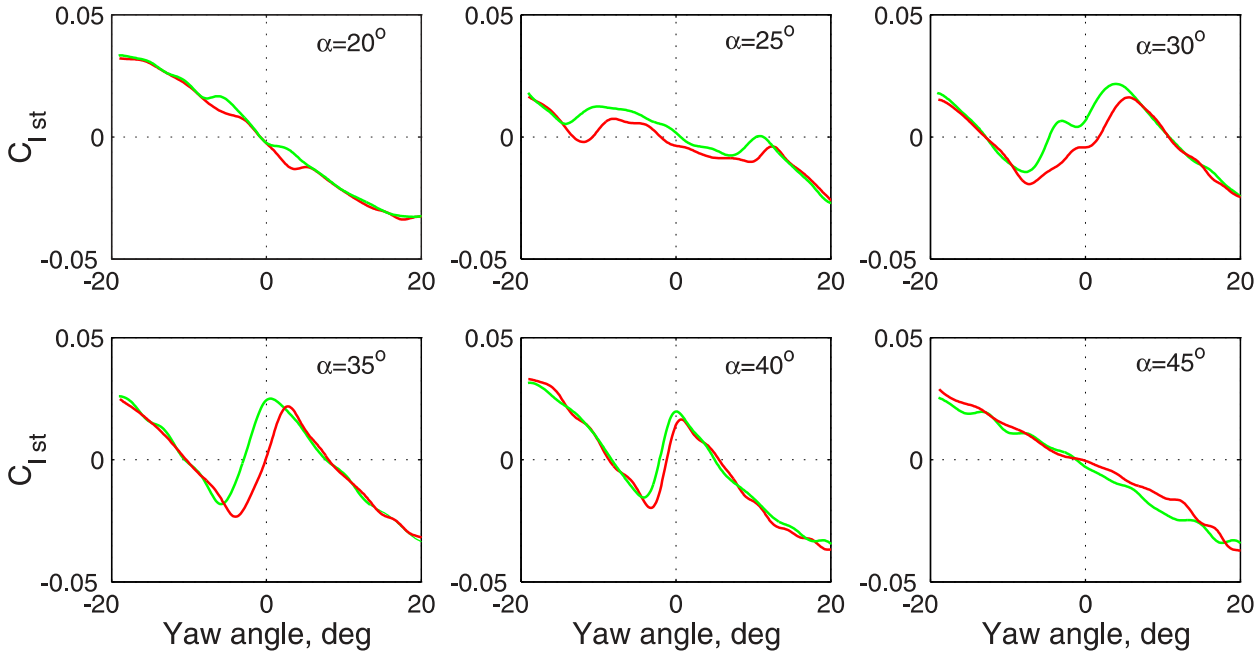

Figure 3. Experimental rolling moment coefficient $C_l(\alpha, \beta)$ for the 65^0 delta wing in slow yaw sweep motion (red lines - $\dot{\beta} = 4$ deg/s, green line $\dot{\beta} = -4$ deg/s).

A sensitivity of the rolling moment even to slow wing motion is high when the vortex breakdown processes dominate and produce a significant aerodynamic contribution. Instead of traditional static tests at different angles of attack and sideslip the 65^0 delta wing has been tested at slow sweep pitch and yaw motion with $\dot{\alpha}, \dot{\beta} \approx \pm 4$ deg/s. The rolling moment coefficient dependencies $C_l(\alpha, \beta)$ are presented in Fig.3, where the red lines correspond to positive yaw rate and the green lines - to negative yaw rate. The hysteresis loops reflect the critical states crossings, when vortex breakdown processes produce significant delays and non-linearities in aerodynamic loads. Based on these slow sweep motion results the static dependencies for the rolling and yawing moment coefficients have been approximated for further mathematical modelling.

The rolling moment coefficient in -phase and out-of-phase aerodynamic derivatives for the 65^0 delta wing with a center body are presented in Figs.4c,d. In the range $\alpha \approx 25 \div 40^0$ they have significant dependence on reduced frequency of oscillation k (or ω). The unsteady aerodynamic responses superimposed on nonlinear static dependence are presented in Fig.4a,b, respectively for $\alpha = 30^0$ and $\alpha = 35^0$. In periodical motion with small amplitude $\Delta\beta = 2.5^0$ at two frequencies $\omega = 0.017$ and $\omega = 0.051$ they have in experiment practically elliptical form, the presented ideal ellipses have been reconstructed from the aerodynamic derivatives. The out-of-phase aerodynamic derivative specifies a size of ellipse-area, while in-phase aerodynamic derivative specifies orientation of ellipse-axis. At small frequencies the ellipse-axis approaches the static dependence slope (green ellipses), and at large frequencies they decline from the static slope significantly (black ellipses). Aerodynamic derivatives in (1) can capture a change of size of ellipse area, but unable to model a change in ellipse orientation, which is in fact an effect of internal flow dynamics.

The considered delta wing without a vertical tail has a very low yawing moment coefficient $C_{n_{st}}$, which is mostly statically unstable with magnitudes only about 10% of the rolling moment coefficient $C_{l_{st}}$.

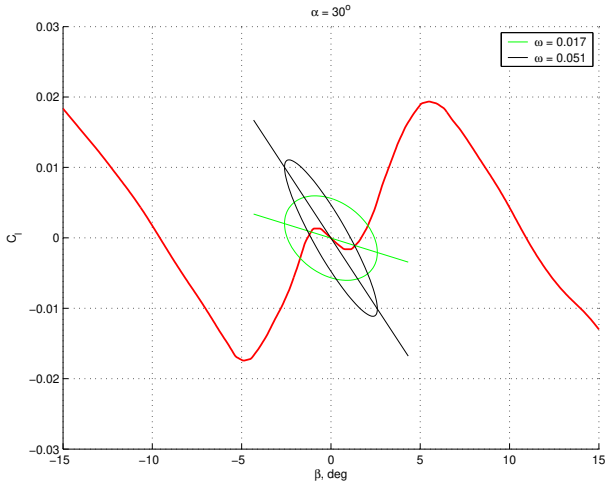

(a) Rolling moment C_l at $\alpha = 30^0$: nonlinear static dependence (red line) and dynamic responses (green line - $k = 0.017$, black line - $k = 0.051$)

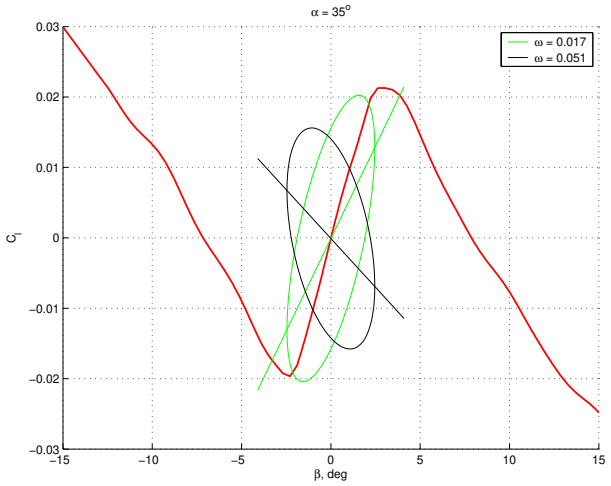

(b) Rolling moment C_l at $\alpha = 35^0$: nonlinear static dependence (red line) and dynamic responses (green line - $k = 0.017$, black line - $k = 0.051$)

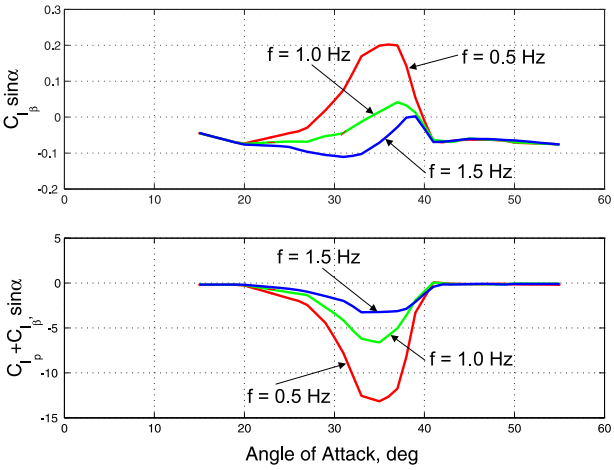

(c) Experimental in-phase and out-of-phase aerodynamic derivatives from oscillations in roll

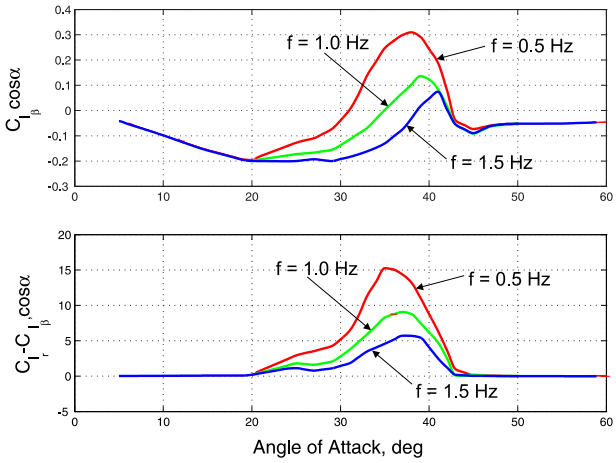

(d) Experimental in-phase and out-of-phase aerodynamic derivatives from oscillations in yaw

Figure 4. Static and dynamic responses in rolling moment coefficient C_l

B. Dynamic representation

1. *Linear model*

To capture the frequency effect in the out-of-phase and in-phase aerodynamic derivatives a simple dynamic model describing unsteady contribution to the full aerodynamic loads can be applied.[8,9]

The rolling moment coefficient during forced roll oscillations can include a separate term for unsteady aerodynamic contribution:

$$C_l = C_{l_{\beta_{att}}}\beta + C_{l_{p_{att}}}\frac{pb}{2V} + C_{l_d}, \tag{2}$$

where $C_{l_{\beta_{att}}}$, $C_{l_{p_{att}}}$ represent aerodynamic derivatives for "hypothetical" attached flow conditions and C_{l_d} describes dynamic contribution from vortical or separated flow. The dynamic contribution C_{l_d} is governed by a linear differential equation:

$$\tau\frac{dC_{l_d}}{dt} + C_{l_d} = C_{l_{\beta_d}}\beta, \tag{3}$$

where τ is the non-dimensional characteristic time scale, term $C_{l_{\beta_d}}\beta$ is the static value of C_{l_d}, $t = 2t'V/b$ is the non-dimensional time, b is the wing span.

All parameters in aerodynamic model (2) and (3) can be identified from the wind tunnel forced oscillation data. In forced roll oscillations the bank angle varies harmonically $\phi = \phi_s \sin\omega t$ and is linked with sideslip angle as $\beta = \phi \sin\alpha_0$.

The in-phase and out-of-phase aerodynamic derivatives are obtained from the forced oscillation data as coefficients of the Fourier series expansion of the measured periodic aerodynamic responses. In accordance with structure of mathematical model (2) and (3) the following connections between the experimental aerodynamic derivatives and parameters of the mathematical model can be derived:

$$\begin{aligned} C_{l_{\beta_{exp}}}(\omega) &= C_{l_{\beta_{att}}}\sin\alpha_0 + \frac{C_{l_{\beta_d}}\sin\alpha_0}{1+\tau^2\omega^2} \\ C_{l_{p_{exp}}}(\omega) &= C_{l_{p_{att}}} - \frac{\tau C_{l_{\beta_d}}\sin\alpha_0}{1+\tau^2\omega^2} \end{aligned} \tag{4}$$

Equations (4) can be transformed to a simple linear relation between the experimental in-phase and out-of-phase aerodynamic derivatives:

$$C_{l_{out}}(\omega) = -\tau C_{l_{in}}(\omega) + a_0, \tag{5}$$

where

$$a_0 = \tau C_{l_{\beta_{att}}}\sin\alpha_0 + C_{l_{p_{att}}}$$

Similar linear connection between aerodynamic derivatives (5) is valid for the experimental data obtained in yaw oscillations. The characteristic time constants and other model parameters can be identified applying to (5) the two-step linear regression method.[9] The linear regression results for the experimental derivatives obtained in roll and yaw oscillations are presented in Fig.5.

The characteristic time constants τ_{roll} and τ_{yaw} in Fig.5,c are identified very accurately at angles of attack $\alpha = 25 \div 35^0$ as the mean square deviations, the vertical bars, are very small. It shows that the model structure fits very well the experimental data. However, in some points the mean square deviation is very high ($\alpha < 25^o$ and $\alpha > 37^0$) because of a reduced frequency effect leading to higher sensitivity to the data errors. Note, that the identified time constants τ_{roll} and τ_{yaw} are very close at $\alpha = 30^0$, and they diverge at higher angles of attack, for example, at $\alpha = 35^0$ the difference is about 30%.

The in-phase and out-of-phase aerodynamic derivatives predicted by mathematical model (2), (3) and experimental ones for shown in Fig.6 demonstrate an excellent agreement. It means that at small amplitude lateral/directional motion the mathematical model will be totally consistent in he time domain with the experimental aerodynamic responses and their dependence on frequency of oscillations.

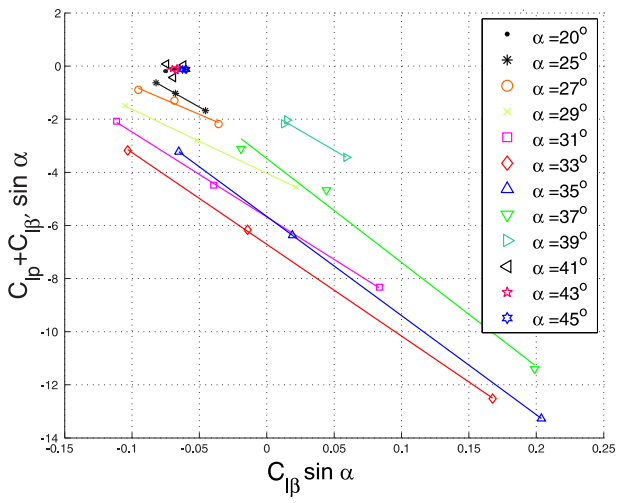

(a) Linear regression of the roll oscillation aerodynamic derivatives

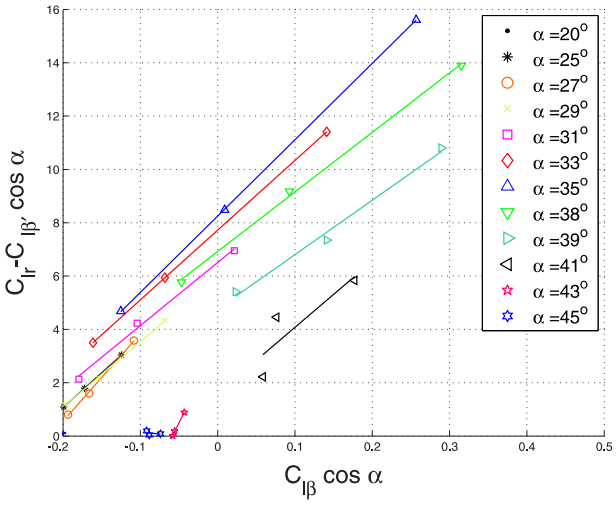

(b) Linear regression of the yaw oscillation aerodynamic derivatives

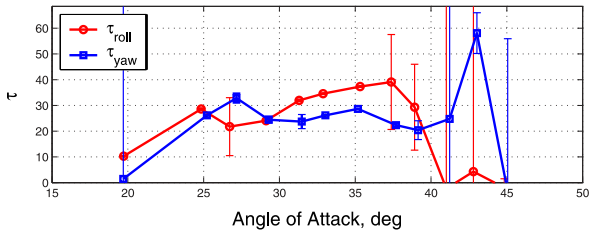

(c) Characteristic time scales identified from the roll and yaw oscillation data

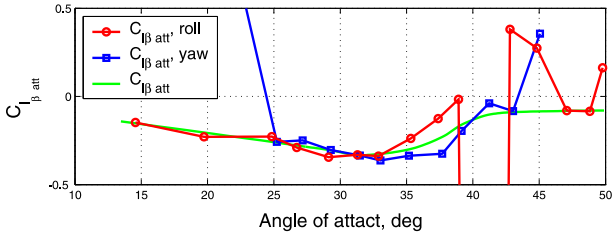

(d) Attached component $Cl_{\beta_{att}}$ identified from the roll and yaw data

Figure 5. Results of the two-step linear regression identification of the aerodynamical model parameters

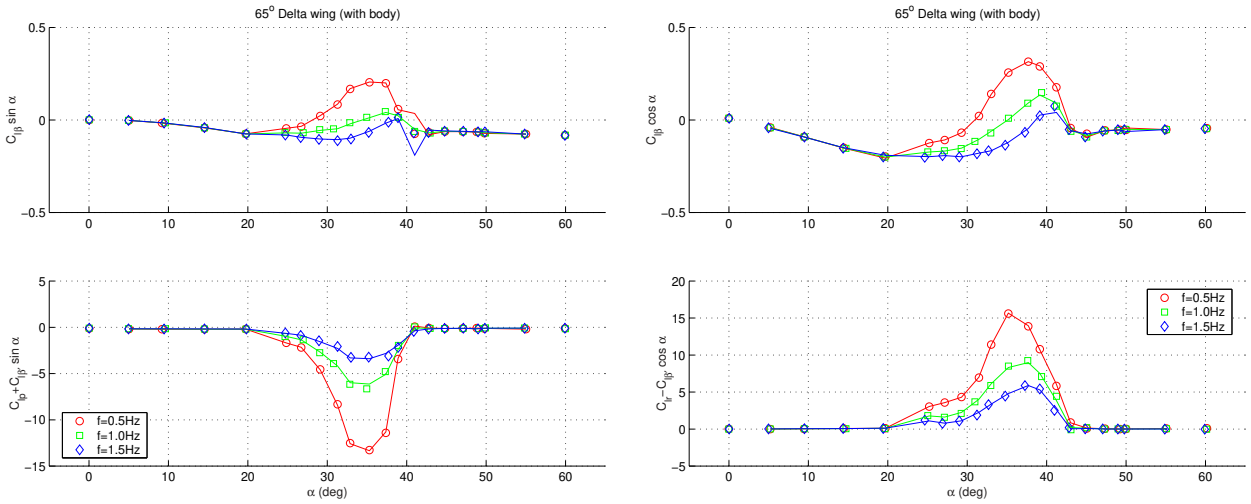

(a) Small amplitude roll oscillation data

(b) Small amplitude yaw oscillation data

Figure 6. The 65^0 delta wing rolling moment coefficient - predicted and experimental dependencies for the in-phase and out-of-phase aerodynamic derivatives.

2. Non-linear model

The linear mathematical model (2),(3) may lose its accuracy at large amplitude oscillations and in vicinity of critical states and static hysteresis loops. To reconcile the mathematical model with these conditions the dynamic equation in (3) is transformed to the nonlinear form:

$$\frac{dC_{l_d}}{dt} = k_0 + k_1\Delta C + k_2\Delta C^2 + k_3\Delta C^3, \tag{6}$$

where $t = \dfrac{2t'V}{b}$ is nondimensional time, $\Delta C(\alpha,\beta) = C_{l_{st}}(\alpha,\beta) - C_{l_{att}}(\alpha,\beta) - C_{l_d}$ and coefficients k_1, k_2, k_3 depend on angle of attack and sideslip $k_i(\alpha,\beta)$.

In the case when $k_0(\alpha,\beta) = k_2(\alpha,\beta) = k_3(\alpha,\beta) = 0$ equation (6) is totally identical to the linear one (3) and the characteristic time scale is linked with k_1 coefficient $\tau = 1/k_1$. If the terms $k_2(\alpha,\beta) \neq 0$, $k_3(\alpha,\beta) \neq 0$ while $k_0(\alpha,\beta) = 0$ equation (6) can model a weak nonlinearity, when an increase in oscillation amplitude is apparent as a change in the time scale τ. Onset of static hysteresis requires $k_0 \neq 0$ and $D = k_2^2 - 4k_3k_1 > 0$.[8,9]

The characteristic time scale $\tau = 1/k_1$ and attached component of the rolling moment derivative $C_{l_{\beta_{att}}}(\alpha)$ have been identified by the two-step linear regression method using small amplitude oscillations data at zero sideslip. They are included in the linearized mathematical model (2),(3) as functions only of angles of attack. Large sideslip angles can require correction of these two parameters due to changes in the flow structure. Their modified forms accounting for sideslip effect is shown in Fig.7. The value τ_{i1} has been identified in the linear model, τ_{i2} and sideslip angles ψ_1, ψ_2, where the characteristic time scales change, have been identified using the large amplitude oscillations in yaw.

The variations of angle of attack and sideslip in the experiment are used as inputs to the mathematical model (2),(6), and mathematical model outputs are compared with the experimental aerodynamic responses.

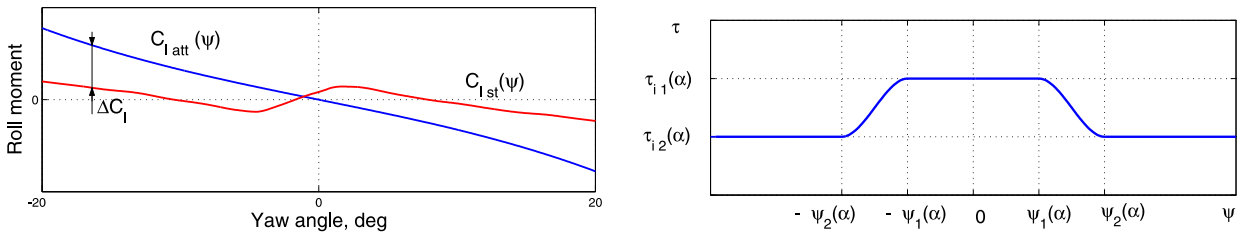

(a) Static and attached dependencies

(b) Characteristic time scale

Figure 7. Non-linear dependence on sideslip angle.

The following positively defined error function is minimized to estimate the unknown model parameters:

$$\Phi_\epsilon = \frac{1}{m(n+1)} \sum_{r=1}^{m} \sum_{i=0}^{n} [C_{r_{exp}} - C_{r_{mod}}]^2, \tag{7}$$

where r is the number of aerodynamic responses, i is the number of sampling points in aerodynamic response time history.

The nonlinear model parameters have been identified in the angle of attack range $\alpha_0 = 20^0 \div 40^0$ with strong nonlinearities in the experimental aerodynamic responses. Without these nonlinear effects the identification of model parameters would be definitely impossible.

Detailed comparison of the aerodynamic responses predicted by the identified nonlinear mathematical model (2), (6) with the experimental aerodynamic responses for $\alpha = 35^0$ are presented in Fig.8 for different reduced frequencies $k = 0.023, 0.046, 0.07$ and two oscillation amplitudes in yaw $\Delta\Psi = 10, 20^0$. Predicted responses $C_{l_{mod}}(t)$ are shown by blue lines, while experimental responses $C_{l_{exp}}(t)$ are shown by yellow squares. The red lines with diamond markers show static dependence $C_{l_{st}}(\beta)$, cyan lines show hypothetical attached flow dependence $C_{l_{att}}(\beta)$ and red lines with triangle markers show the difference between the static dependence and the attached one $C_{l_{st}}(\beta) - C_{l_{att}}(\beta)$. Magenta solid lines show variation of dynamic variable $C_{l_d}(t)$. Presented comparison shows rather good agreement between the mathematical model aerodynamic responses and experimental aerodynamic responses both qualitatively and quantitatively.

III. Aircraft lateral/directional dynamics at high incidence

In the conceptual and preliminary aircraft design stage simple methods and criteria based on static stability and control characteristics have been widely used in engineering practice to estimate manoeuvre boundaries at high incidence flight.[10] The directional departure parameter $C_{n_{\beta_{dynamic}}} = C_{n_\beta} - \frac{I_z}{I_x} C_{l_\beta} \sin\alpha$, the Lateral Control Departure Parameter LCDP=$C_{n_\beta}\left(1 - \frac{C_{l_\beta}}{C_{n_\beta}} \frac{C_{n_{\delta_a}}}{C_{l_{\delta_a}}}\right)$, the damping-in-roll parameter $C_{l_p} + C_{l_{\dot\beta}} \sin\alpha$ have been effectively used in the past for prediction of departures and wing-rock onset.

Modern and future aircraft are potentially able to fly at high angles of attack due to introduction of thrust vectoring and digital automatic control technologies. However, the design of control system, which will maintain stable and controllable flight beyond stall conditions, requires an accurate knowledge of the nonlinear and unsteady aerodynamic characteristics over a large range of α, β.

The unsteady aerodynamic models presented in the previous section take into account the time lag effects produced by separated flow dynamics and thus incorporate dependence on oscillation frequency or in fact on motion prehistory.

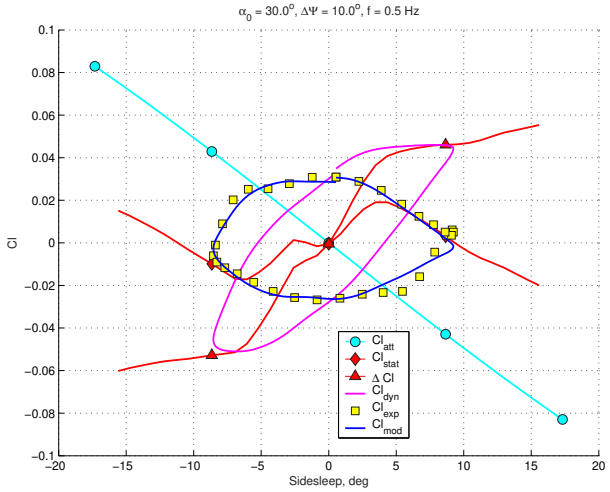

(a) $\Delta\Psi = 10^0$, $k = 0.023$

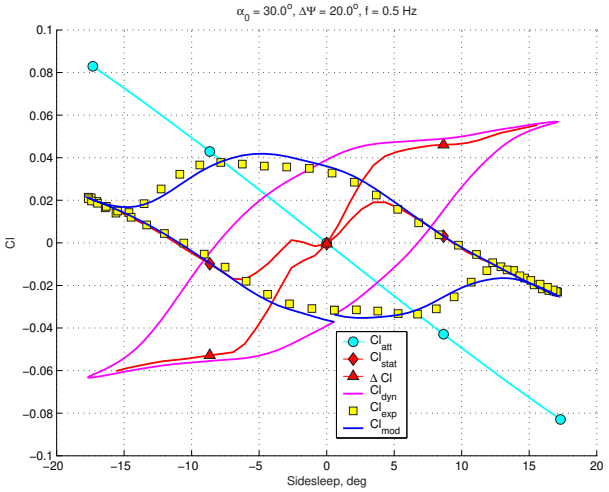

(b) $\Delta\Psi = 20^0$, $k = 0.023$

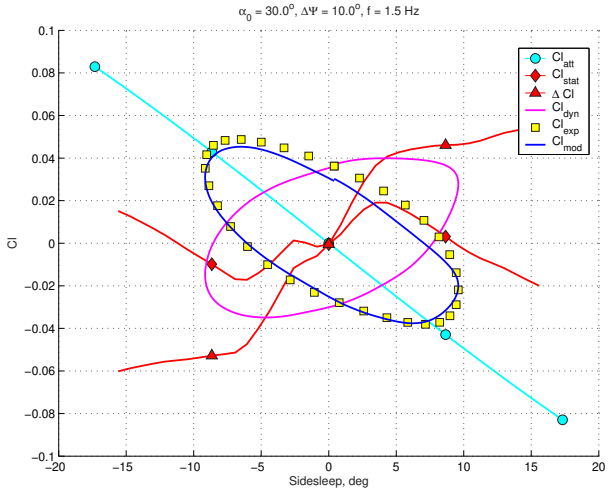

(c) $\Delta\Psi = 10^0$, $k = 0.07$

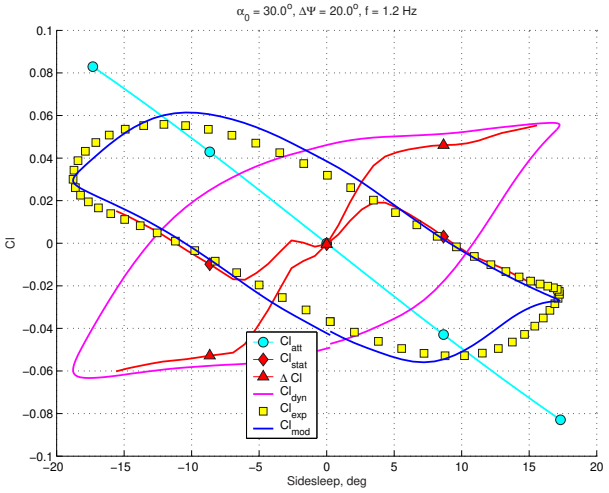

(d) $\Delta\Psi = 20^0$, $k = 0.07$

Figure 8. Rolling moment coefficient C_l - predicted and experimental aerodynamic responses at large amplitudes oscillations in yaw.

The current practice is mostly based on application of aerodynamic derivatives representation for high angles of attack simulation and control design. The main objective of this paper is to show the difference in terms of the open- and closed-loop stability characteristics of the lateral/directional motion if a more adequate aerodynamic model will be applied.

We will consider small amplitude lateral/directional motion and suppose that this dynamics is decoupled from the longitudinal dynamics. The only dependence from longitudinal dynamics will be trimmed angle of attack α_0. This angle of attack is trimmed in level flight at some given altitude H and Mach number by aerodynamic or thrust vectoring control as it is shown in.[11]

A. Lateral/directional motion equations

For the lateral/directional motion control we will use the thrust vectoring in yaw δ_{T_ψ} (see Fig.2, a) and ailerons δ_a. The aileron control derivatives $C_{l_{\delta_a}}$ are $C_{n_{\delta_a}}$ for the 65^0 delta wing are available from the wind tunnel tests conducted in TsAGI.

In dynamic analysis we will consider the following linearized lateral/directional equations of motion:

$$\begin{aligned}
\frac{d\beta}{dt} &= p\sin\alpha_0 - r\cos\alpha_0 + \frac{-T\delta_{T_\psi} + \bar{q}SC_y}{mV} + \frac{g}{V}\cos\alpha_0\phi \\
\frac{dp}{dt} &= \frac{\bar{q}Sb}{I_x}C_l \\
\frac{dr}{dt} &= \frac{\bar{q}Sb}{I_z}C_n + \frac{TR_T}{I_z}\delta_{T_\psi} \\
\frac{d\phi}{dt} &= p + r\tan\alpha_0,
\end{aligned} \tag{8}$$

where the side force, the rolling and yawing moment coefficients will be used in two different forms - based on the aerodynamic derivative concept and based on partitioning and dynamic representation of vortical flow contribution in the full aerodynamic loads.

B. Aerodynamic coefficients representation

The **first form** of aerodynamic coefficients representation is based on aerodynamic derivative concept and has the following form:

$$\begin{aligned}
C_y &= C_{y_{\beta_{fo}}}(\alpha_0,k)\beta + C_{y_{p_{fo}}}(\alpha_0,k)\frac{pb}{2V} + C_{y_{r_{fo}}}(\alpha_0,k)\frac{rb}{2V} + C_{y_{\delta_a}}(\alpha_0)\delta_a \\
C_l &= C_{l_{\beta_{fo}}}(\alpha_0,k)\beta + C_{l_{p_{fo}}}(\alpha_0,k)\frac{pb}{2V} + C_{l_{r_{fo}}}(\alpha_0,k)\frac{rb}{2V} + C_{l_{\delta_a}}(\alpha_0)\delta_a \\
C_n &= C_{n_{\beta_{fo}}}(\alpha_0,k)\beta + C_{n_{p_{fo}}}(\alpha_0,k)\frac{pb}{2V} + C_{n_{r_{fo}}}(\alpha_0,k)\frac{rb}{2V} + C_{n_{\delta_a}}(\alpha_0)\delta_a,
\end{aligned} \tag{9}$$

where the aerodynamic derivatives obtained in forced oscillation tests in roll and yaw as a combination of rotary and unsteady aerodynamic derivatives depend on angle of attack α_0 and reduced frequency parameter $k = \dfrac{\omega b}{2V}$.

The **second form** for representation of aerodynamic coefficients is based on aerodynamic loads parti-

tioning and dynamic modelling of flow time lag effects. It has the following form:

$$
\begin{aligned}
C_y &= C_{y_{\beta_{att}}}(\alpha_0)\beta + C_{y_{p_{att}}}(\alpha_0)\frac{pb}{2V} + C_{y_{r_{att}}}(\alpha_0)\frac{rb}{2V} + C_{y_{\delta_a}}(\alpha_0)\delta_a + C_{y_d} \\
C_l &= C_{l_{\beta_{att}}}(\alpha_0)\beta + C_{l_{p_{att}}}(\alpha_0)\frac{pb}{2V} + C_{l_{r_{att}}}(\alpha_0)\frac{rb}{2V} + C_{l_{\delta_a}}(\alpha_0)\delta_a + C_{l_d} \\
C_n &= C_{n_{\beta_{att}}}(\alpha_0)\beta + C_{n_{p_{att}}}(\alpha_0)\frac{pb}{2V} + C_{n_{r_{att}}}(\alpha_0)\frac{rb}{2V} + C_{n_{\delta_a}}(\alpha_0)\delta_a + C_{n_d},
\end{aligned}
\tag{10}
$$

where aerodynamic derivatives $C_{y_{\beta_{att}}}$, $C_{l_{p_{att}}}$, $C_{n_{r_{att}}}$, etc. corresponding to attached flow conditions do not depend on reduced frequency k and dynamic contributions from vortical flow C_{y_d}, C_{l_d}, C_{n_d} are described by the following dynamic equations:

$$
\begin{aligned}
\frac{\tau_{c_y} b}{2V}\frac{dC_{y_d}}{dt} + C_{y_d} &= C_{y_{\beta_d}}(\alpha_0)\beta \\
\frac{\tau_{c_l} b}{2V}\frac{dC_{l_d}}{dt} + C_{l_d} &= C_{l_{\beta_d}}(\alpha_0)\beta \\
\frac{\tau_{c_n} b}{2V}\frac{dC_{n_d}}{dt} + C_{n_d} &= C_{n_{\beta_d}}(\alpha_0)\beta
\end{aligned}
\tag{11}
$$

C. State-space dynamic models

Combining (8) and (9) we can represent the equations for the lateral/directional motion with aerodynamic derivatives formulation in the state space form:

$$
\dot{\mathbf{x}} = A\mathbf{x} + B\mathbf{u}, \tag{12}
$$

where $\mathbf{x} = (\beta, p, r, \phi)^T$, $\mathbf{u} = (\delta_{T_\psi}, \delta_a)^T$ and

$$
A = \begin{Vmatrix}
\frac{\bar{q}S}{mV}C_{y_{\beta_{fo}}}(\alpha_0,k) & \sin\alpha_0 & -\cos\alpha_0 & \frac{g}{V}\cos\alpha_0 \\
\frac{\bar{q}Sb}{I_x}C_{l_{\beta_{fo}}}(\alpha_0,k) & \frac{\bar{q}Sb^2}{2I_xV}C_{l_{p_{fo}}}(\alpha_0,k) & \frac{\bar{q}Sb^2}{2I_xV}C_{l_{r_{fo}}}(\alpha_0,k) & 0 \\
\frac{\bar{q}Sb}{I_z}C_{n_{\beta_{fo}}}(\alpha_0,k) & \frac{\bar{q}Sb^2}{2I_zV}C_{n_{p_{fo}}}(\alpha_0,k) & \frac{\bar{q}Sb^2}{2I_zV}C_{n_{r_{fo}}}(\alpha_0,k) & 0 \\
0 & 1 & \tan\alpha_0 & 0
\end{Vmatrix}
$$

$$
B = \begin{Vmatrix}
-\frac{T}{mV} & 0 \\
0 & \frac{\bar{q}Sb}{I_x}C_{l_{\delta_a}}(\alpha_0) \\
\frac{TR_T}{I_z} & \frac{\bar{q}Sb}{I_z}C_{n_{\delta_a}}(\alpha_0) \\
0 & 0
\end{Vmatrix}
\tag{13}
$$

Combining (8) and (10),(11) we can represent equations for the lateral/directional motion with dynamic aerodynamic model also in the state space form (12), where $\mathbf{x} = (\beta, p, r, \phi, C_{l_d}, C_{n_d})^T$ and $\mathbf{u} = (\delta_{T_\psi}, \delta_a)^T$ (the dynamic contribution in the side force is neglected).

In this case matrices A and B have the following representation:

$$A = \begin{Vmatrix} \frac{\bar{q}S}{mV} C_{y_{\beta_{att}}}(\alpha_0) & \sin\alpha_0 & -\cos\alpha_0 & \frac{g}{V}\cos\alpha_0 & 0 & 0 \\ \frac{\bar{q}Sb}{I_x} C_{l_{\beta_{att}}}(\alpha_0) & \frac{\bar{q}Sb^2}{2I_xV} C_{l_{p_{att}}}(\alpha_0) & \frac{\bar{q}Sb^2}{2I_xV} C_{l_{r_{att}}}(\alpha_0) & 0 & \frac{\bar{q}Sb}{I_x} & 0 \\ \frac{\bar{q}Sb}{I_z} C_{n_{\beta_{att}}}(\alpha_0) & \frac{\bar{q}Sb^2}{2I_zV} C_{n_{p_{att}}}(\alpha_0) & \frac{\bar{q}Sb^2}{2I_zV} C_{n_{r_{att}}}(\alpha_0) & 0 & 0 & \frac{\bar{q}Sb}{I_z} \\ 0 & 1 & \tan\alpha_0 & 0 & 0 & 0 \\ \frac{2V}{\tau_{c_l} b} C_{l_{\beta_d}}(\alpha_0) & 0 & 0 & 0 & -\frac{2V}{\tau_{c_l} b} & 0 \\ \frac{2V}{\tau_{c_n} b} C_{n_{\beta_d}}(\alpha_0) & 0 & 0 & 0 & 0 & -\frac{2V}{\tau_{c_n} b} \end{Vmatrix} \tag{14}$$

$$B = \begin{Vmatrix} -\frac{T}{mV} & 0 \\ 0 & \frac{\bar{q}Sb}{I_x} C_{l_{\delta_a}}(\alpha_0) \\ \frac{TR_T}{I_z} & \frac{\bar{q}Sb}{I_z} C_{n_{\delta_a}}(\alpha_0) \\ 0 & 0 \\ 0 & 0 \\ 0 & 0 \end{Vmatrix}$$

For large amplitude simulation of the lateral/directional dynamics nonlinear aerodynamic models for the rolling moment coefficient C_l and yawing moment coefficient C_n in the form (6) will be used. In this case equations (14) are added by nonlinear term:

$$\dot{\mathbf{x}} = A\mathbf{x} + B\mathbf{u} + f(\mathbf{x}), \tag{15}$$

IV. Open-loop and closed-loop dynamic analysis of lateral/directional motion at high incidence flight

The open- and closed-loop lateral/directional dynamics at high angles of attack is analyzed considering two types of aerodynamic representation, namely, using system (13) and system (14). In the first case reduced frequency k is considered as a parameter and its effect is analysed.

A. Open-loop analysis

The eigenvalues of the linearized lateral/directional motion equations in the form (14) and (13) for different four angles of attack $\alpha_0 = 25,\ 30,\ 35,\ 40^0$ are shown in Fig.9.

System (14) for the dynamic aerodynamic model has six eigenvalues, they are marked by black circles. Four eigenvalues for the aerodynamic derivatives model (system (13)) are marked by red, green and blue crosses for $k = 0.026,\ 0.046,\ 0.0702$, respectively.

The Dutch-roll mode eigenvalues in system (14) exist with rather high frequency $\omega \approx 2$ 1/s at all considered angles of attack. In system (13) with conventional aerodynamic model the Dutch-roll mode eigenvalues exist only at $\alpha_0 = 25^0$ - $\omega \approx 1.5s^{-1}$. At $\alpha_0 = 30 \div 40^0$ all eigenvalues in (13) are concentrated close to the real axis.

At $\alpha > 30^0$ the both systems become aperiodically unstable, the roll mode eigenvalues move to the right semiplane, however, the level of aperiodic instability is higher for system (14), when more adequate unsteady aerodynamic model is taken into account.

The difference in location of the Dutch roll and roll-subsidence modes eigenvalues in system (14) is due to coupling of the lateral/directional modes eigenvalues with unsteady aerodynamic. These two negative real eigenvalues are located very close to eigenvalues of the lateral/directional modes eigenvalues. For example, at $\alpha_0 = 20^0$ the unsteady aerodynamic eigenvalues equal $s_{u_1} = -2.7s^{-1}$ and $s_{u_2} = -1.4s^{-1}$ and at $\alpha_0 = 35^0$ they are much smaller $s_{u_1} = -0.3s^{-1}$ and $s_{u_2} = -0.2s^{-1}$.

Effect of reduced frequency parameter k on eigenvalues of system (13) is more significant on the ends of the considered angle of attack interval at $\alpha = 25^0$ and $\alpha = 40^0$.

Comparative analysis of the open-loop eigenvalues with two types of aerodynamic representation shows that account of adequate unsteady aerodynamic effects (14) leads at $\alpha > 33^0$ to a higher level of aperiodic instability. System (14) also has the stable Ducth roll complex pair at all angels of attack, while in system (13) the oscillatory mode practically disappears at $\alpha > 28^0$.

A significant difference in eigenvalues location for aerodynamic derivatives model (13) with respect to more adequate unsteady aerodynamic model will make practically impossible design of control laws stabilizing the lateral/directional aircraft motion, when aerodynamic derivatives model is implemented.

B. Closed-loop analysis

To maintain stable flight at high angles of attack stabilizing control laws should be not only stable locally, but also provide reasonable stability at large disturbances. As shown in Fig.3 the rolling moment at high incidence has very nonlinear dependence on sideslip, which is the result of vortex breakdown processes above the wing.

Linearly designed control law can fail at large amplitude disturbed motion and will be unable to suppress wing-rock motion, the large amplitude stable oscillations in roll and yaw, which are typical at high angle of attack for many modern aircraft. The nonlinear stabilization of the lateral/directional motion at high incidence flight in the range $\alpha = 35 \div 40^0$ is rather complicated problem due to unsteady and nonlinear nature of the aerodynamic loads and we will not consider this problem in this paper.

1. Stabilizing control laws

Two linear control design techniques are considered for stabilization of the linearized lateral/directional dynamics: the LQ-optimal and the pole placement methods.

The state vector in (12) for aerodynamic derivative model $x = (\beta, p, r, \phi)^T$ can be measured by standard sensors and so are totally observable, while in the case of unsteady aerodynamic model $x = (\beta, p, r, \phi, C_{l_d}, C_{n_d})^T$ two internal unsteady aerodynamic variables C_{l_d}, C_{n_d} can not be directly measured. So, the measurement vector

$$y = Cx$$

in these two cases has the same dimension, matrix $C \in R^{4\times 6}$ for unsteady aerodynamic model, and $C \in R^{4\times 4} = I_4$ for aerodynamic derivative model.

The control vector $u = (\delta_{T_\psi}, \delta_{\delta_a})^T$ including thrust and aileron deflection has amplitude and deflection rate limits:

$$|\delta_{T_\psi}| \le u_{max_1},\ |\delta_a| \le u_{max_2},$$

$$|\dot{\delta}_{T_\psi}| \le \dot{u}_{max_1},\ |\dot{\delta}_a| \le \dot{u}_{max_2},$$

where $u_{max_1} = u_{max_2} = 20^0$, $\dot{u}_{max_1} = \dot{u}_{max_2} = 50\, o/s$.

The open-loop lateral/directional motion are periodically unstable at $\alpha > 34^0$ considering both aerodynamic models, and in the case of unsteady aerodynamic model the level of instability is higher.

Stabilization of unstable system with constrained control has some specific problems.[13] An unstable linear system under control constraints has bounded controllable region, in which the stabilization problem can be solved. As a result, this linear system may not be globally stabilizable.

The controllable region is the set of states that can be steered to the origin with available bounded control. Its size can serve as a metric showing the complexity of the stabilization problem. If the controllability region size is very small it indicates the need in more powerful control effectors. In our study for computation of controllability regions we implement the algorithm from,[14] taking into account the amplitude and deflection rate limits.

The closed-loop system with any control law will have attraction region, which size will be less or equal to the size of controllability region of the open-loop system. A relative size of the attraction region can be considered as an additional indicator for the closed loop system.

2. Observer and LQR design

To stabilize the unstable system with one positive real value a controller must know the states of unstable subsystem. But it is practically impossible without two unsteady aerodynamic variables.

Unmeasurable variables C_{l_d}, C_{n_d} can be obtained using the Kalman estimator in the form:

$$\dot{x}_e(t) = Ax_e(t) + Bu(t) + L(y(t) - Cx_e(t)),$$

so that the feeback controller can be now designed with estimated full vector

$$u(t) = Kx_e(t).$$

The estimator gain L is obtained using function *kalman* MATLAB Control System Toolbox[15] with the following parameters:

$$Q_n = I, R_n = I.$$

The state feedback gain matrix for the linear quadratic regulator

$$K = -B^T P.$$

needs matrix P, which is the unique positive solution of the following Riccati equation:

$$A^T P + PA - P^T BB^T P = 0,$$

where A and B are matrices of the linear system (12).

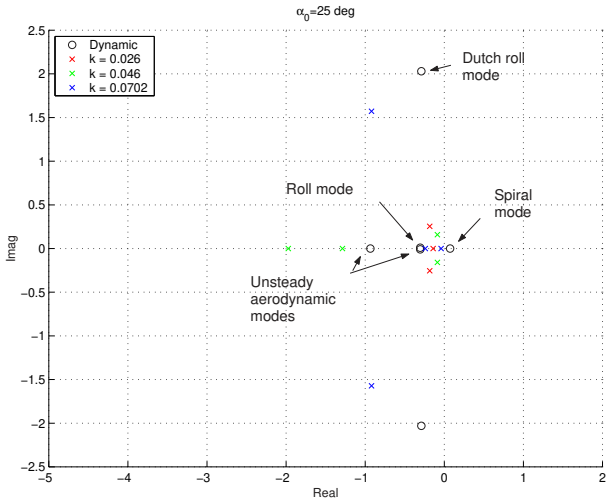

(a) $\alpha_0 = 25^0$

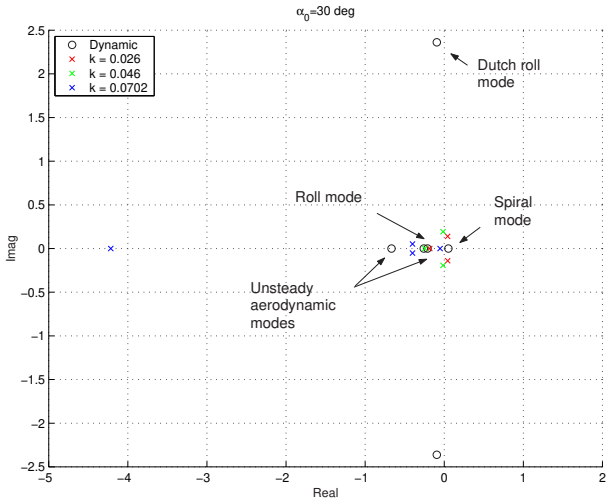

(b) $\alpha_0 = 30^0$

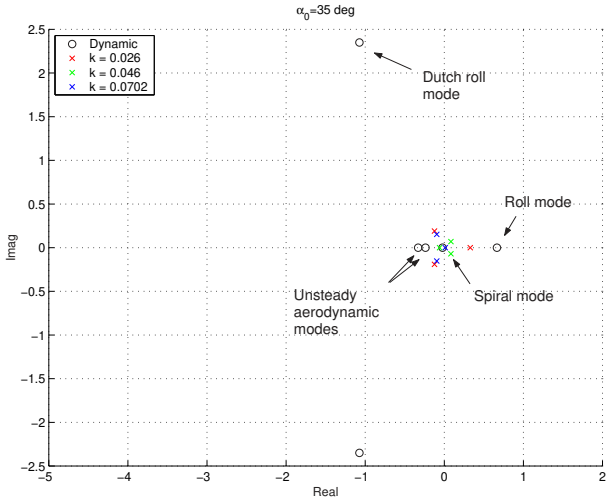

(c) $\alpha_0 = 35^0$

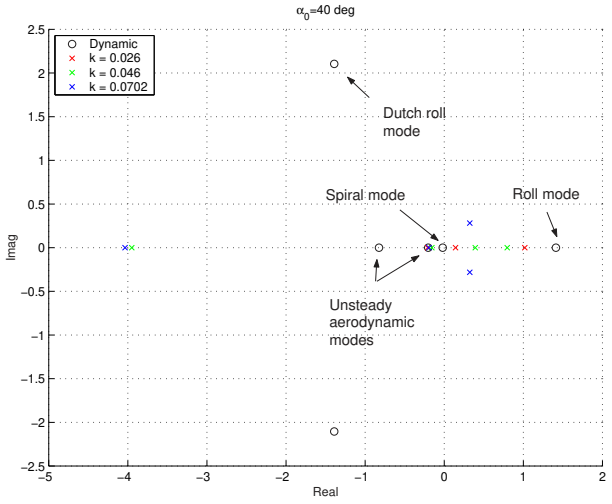

(d) $\alpha_0 = 40^0$

Figure 9. Open-loop system eigenvalues in level flight at $H = 1$ km. Black circles - system (14), red, green and blue crosses - system (13) for $k = 0.026, 0.046, 0.07$, respectively.

3. *Comparison of LQ and pole placement controllers*

The closed-loop system stability region or domain of attraction depends on applied controller. To illustrate this fact the designed LQ-optimal controller was compared with the pole placement control law, which was obtained via function *place* from MATLAB Control System Toolbox.

At $\alpha_0 = 40^0$ the following closed-loop poles were chosen to provide the closed-loop system satisfactory dynamics:

Unsteady aerodynamic model	Aerodynamic derivative model
$-0.49 + 2.1i$	$-0.49 + 2.1i$
$-0.49 - 2.1i$	$-0.49 - 2.1i$
-1.41	-1.41
-0.02	-0.02
-1.202	
-1.825	

The boundaries of controllability regions and domain of attractions in different cross sections are presented in Figs. 10 and 11. Domain of attractions have been obtained by direct numerical integration of the closed-loop system under saturated control laws with a number of initial conditions taken inside the controllable region.

The controllability region with aerodynamic control δ_a is very small and unsatisfactory, while in combination with thrust vectoring δ_{T_ψ}, the controllability region size expands significantly (see Fig.10, a). Effect of the rate limit $\dot{\delta}_{T_\psi}^{max} = 50 deg/s$ in thrust vectoring on the size of controllability region is not very significant (see Fig.10, b).

As it was expected,[13] the domain of attraction for the LQ-optimal controller is much bigger and covers a large part of controllable region, while the controllability region for the pole placement control law is quite small and therefore unsatisfactory (see Fig.10, c,d).

In the case of aerodynamic derivative model the domain of attraction for the LQ-optimal controller covers all states in the controllable region. The result for the unsteady aerodynamic model (see Fig. 10) is worse due to incorporated into the control system observer. In both cases, the minimum energy LQ-optimal controller outperforms the pole placement control law in terms of size of domain of attraction, which is the critical factor in control design for inherently unstable dynamics.

Analysis of the closed-loop dynamics of the linearized lateral/directional system has highlighted the problem in design of stabilizing control laws in terms of the stability region size. The application of the LQ-optimal controller provides reasonably good results if the size of controllable region is sufficient to reject external disturbances.

When control law affects also the stable subspace of the system in order to shape the lateral/directional dynamics with handling quality requirements the size of the closed-loop system stability region may become very small.

The design of stabilizing control law for the lateral/directional motion at high angles of attack is much more complicated that we considered above. In reality the rolling and yawing moment coefficients are essentially nonlinear in sideslip (see Fig.4) and have significant time lag effects due to flow dynamics. The control design in such conditions needs special approach and investigation.

Conclusions

Comparative analysis of two forms of aerodynamic representation, the dynamic unsteady aerodynamic model and the conventional model based on aerodynamic derivatives concept, in terms of their impact on the lateral/directional stability characteristics and control design issues shows, that:

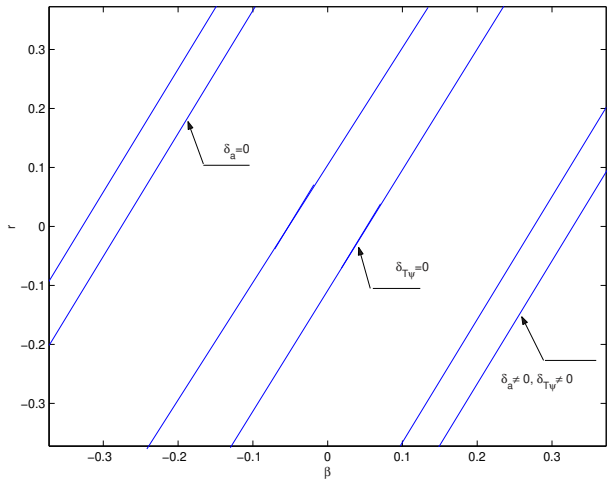

(a) Effect of thrust vectoring - slice in the plane (β, p)

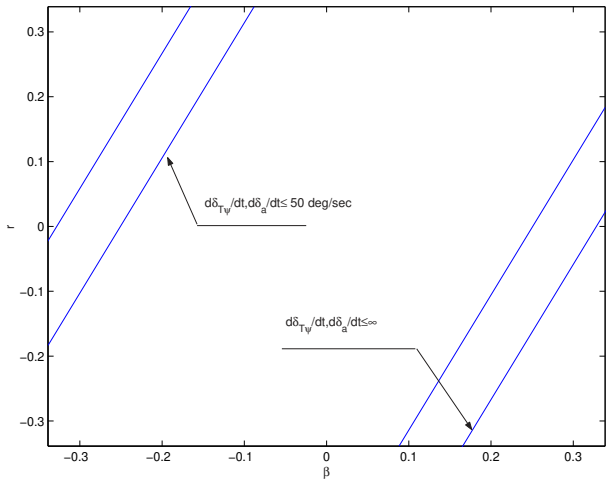

(b) Effect of thrust vectoring - slice in the plane (β, r)

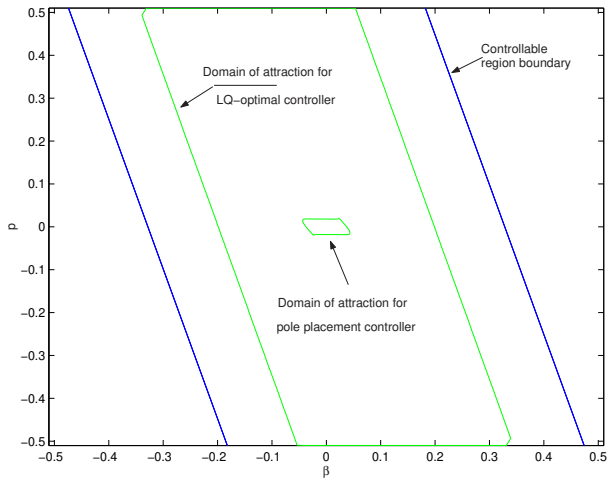

(c) Comparison of LQR and pole placement - slice in the plane (β, p)

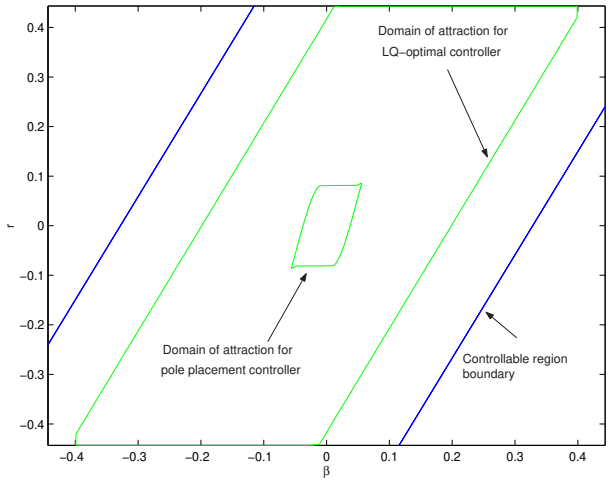

(d) Comparison of LQR and pole placement - slice in the plane (β, r)

Figure 10. Open-loop controllablity and closed-loop stability regions for unsteady aerodynamic model.

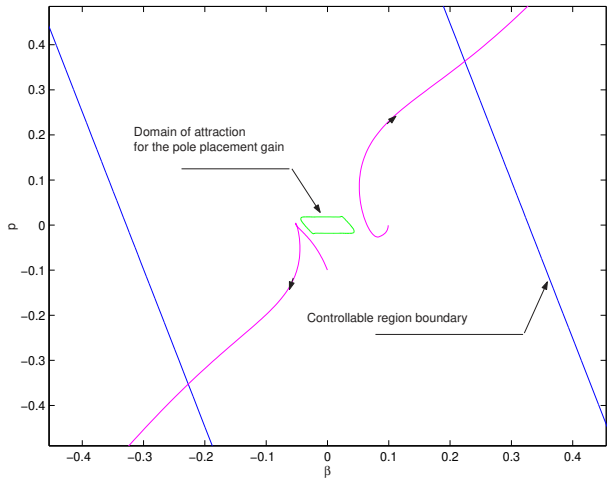

(a) Pole placement - slice in the plane (β, p)

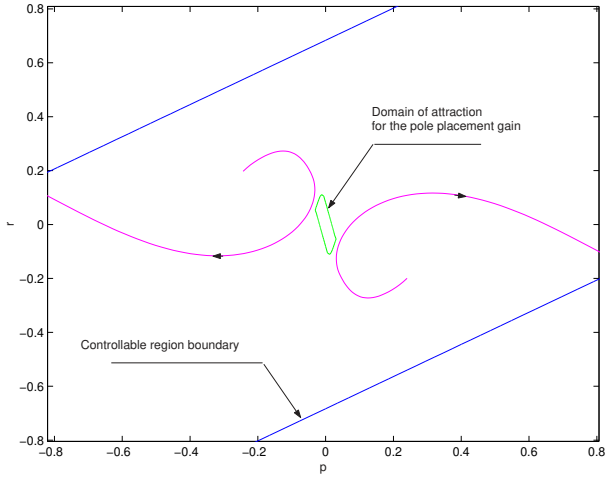

(b) Pole placement - slice in the plane (p, r)

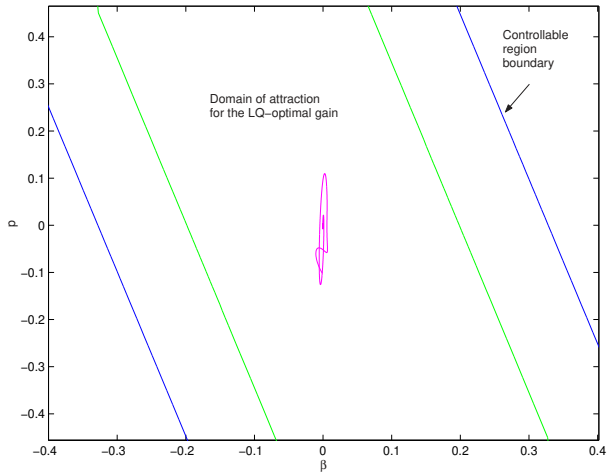

(c) LQR - slice in the plane (β, p)

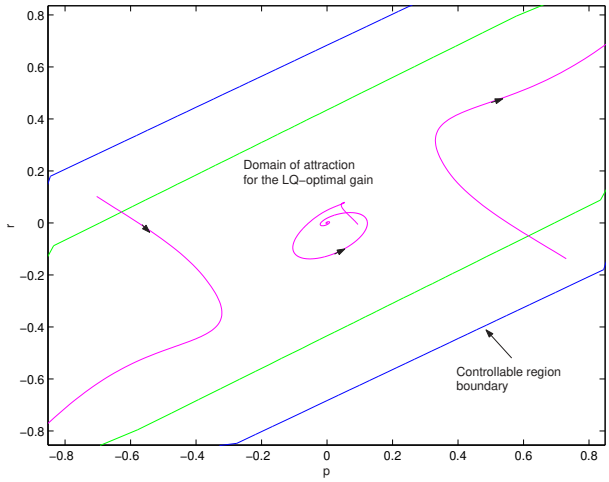

(d) LQR - slice in the plane (p, r)

Figure 11. Open-loop controllability and closed-loop stability regions for unsteady aerodynamic model.

- at high angles of attack conditions the unsteady aerodynamic model taking into account the time lag effects produced by flow dynamics is more adequate for flight dynamics analysis and control design,

- the conventional aerodynamic derivative model beyond the stall conditions can not provide accurate prediction of stability characteristics and be applied for control design,

- special attention should be given during control design to the closed-loop system stability region size, aerodynamic control at high angles of attack at the presence of control constraints is effective only in combination with thrust vectoring.

Acknowledgement

This work has been funded in part by QinetiQ Ltd, UK and monitored by Doug Greenwell and George Nichols. The authors are gratefully acknowledge this support.

References

[1]Greenwell, D.I. "Difficulties in the Application of Stability Derivatives to the Manoeuvring Aerodynamics of Combat Aircraft," ICAS Paper 98-1.7.1, the 21th Congress of the Aeronautical Sciences, Sept. 1998, Melbourne, Australia.

[2]Tobak, M. and Schiff, L.B. "On the Formulation of the Aerodynamic Characteristics in Aircraft Dynamics," NASA TR-R-456, 1976.

[3]Rohlf, R., Brieger, O., and Th. Grohs "X-31 VECTOR Control Law Design for ESTOL to the Ground," AIAA Guidance, Navigation, and Control Conference and Exibit, 11-14 August 2003, Austin, Texas.

[4]Smith, M.S., "Analysis of Wind Tunnel Oscillatory Data of the X-31A Aircraft", NASA/CR-1999-208725, Feb. 1999.

[5]Goman, M.G., and A.N.Khrabrov. "State-Space Representation of Aerodynamic Characteristics of an Aircraft at High Angles of Attack," Journal of Aircraft, Vol.31, No.5, Sept.-Oct. 1994, pp.1109 - 1115.

[6]Klein, V., and Noderer, K.D. "Modeling of Aircraft Unsteady Aerodynamic Characteristics," Part 1 - Postulated Models, NASA TM 109120, May 1994; Part 2 - Parameters Estimated From Wind Tunnel Data, NASA TM 110161, April 1995; Part 3 - Parameters Estimated From Flight Data, NASA TM 110259, May 1996.

[7]Myatt, J.H., "Multiple Time-Scale Effects for a Pitching 65^o Delta Wing," Paper 98-4354, AIAA Atmosperic Flight Mechanics Conference, August 1998, Boston MA.

[8]Abramov, N.B., Goman, M.G., Khrabrov, A.N., and K.A.Kolinko "Simple Wings Unsteady Aerodynamics at High Angles of Attack: Experimental and Modeling Results," Paper 99-4013, AIAA Atmospheric Flight Mechanics Conference, August 1999, Portland, OR.

[9]Abramov, N., Goman, M., Greenwell, D., and A. Khrabrov. "Two-Step Linear Regression Method for Identification of High Incidence Unsteady Aerodynamic Model", Paper 2001-4080, AIAA Atmospheric Flight Mechanics Conference, August 2001, Montreal, Canada.

[10]Manoeuvre Limitations of Combat Aircraft. AGARD-AR-155A, 1979.

[11]Abramov, N., Goman,M., and A. Khrabrov. "Aircraft Dynamics at High Incidence Flight with Account of Unsteady Aerodynamic Effects ", AIAA-2004-5274, AIAA Atmospheric Flight Mechanics Conference and Exhibit, Providence, Rhode Island, Aug. 16-19, 2004

[12]Dorsett,K.M., Fears, S.P., and H.P.Houlden "Innovative Control Effectors (ICE). Phase II", WL-TR-97-3059, August 1997.

[13]T. Hu and Z. Lin. *Control systems with actuator saturation: analysis and design*. Boston: Birkhäuser, 2001.

[14]Goman, M.G., and M.N. Demenkov. "Computation of Controllability Regions for Unstable Aircraft Dynamics," Journal of Guidance, Control, and Dynamics, Vol.27, No.4, July-August 2004.

[15]*MATLAB Control System Toolbox User's Guide*. The MathWorks, 1999.